Light-induced magnetization changes in aggregated and isolated cobalt ferrite nanoparticles

Tatiana V. Brinzari, Divya Rajan, Cauê F. Ferreira, Sebastian A. Stoian, Pedro A. Quintero, Mark W. Meisel, and Daniel R. Talham

---

Articles you may be interested in

Light-induced magnetization changes in aggregated and isolated cobalt ferrite nanoparticles

Tatiana V. Brinzari,[1,a)] Divya Rajan,[2,a)] Cauê F. Ferreira,[2] Sebastian A. Stoian,[3,4] Pedro A. Quintero,[1] Mark W. Meisel,[1,b)] and Daniel R. Talham[2,c)]

[1]*Department of Physics and National High Magnetic Field Laboratory, University of Florida, Gainesville, Florida 32611-8440, USA*
[2]*Department of Chemistry, University of Florida, Gainesville, Florida 32611-7200, USA*
[3]*National High Magnetic Field Laboratory, Florida State University, Tallahassee, Florida 32310-3706, USA*
[4]*Department of Chemistry, University of Idaho, Moscow, Idaho 83844-2343, USA*

The light-induced magnetization changes in cobalt ferrite nanoparticles are reinvestigated to probe the mechanism of photomagnetic behavior and to uncover the essential criteria required to observe the effect. Irradiation with white light results in pronounced demagnetization as evidenced by a decrease in the coercivity ($\Delta H_c \sim 3$ kOe at 10 K) and a drop in the high field magnetization at 70 kOe. Wavelength dependent studies show the optical excitation driving the effect is broad in nature. Power and temperature (T) dependent measurements reveal strikingly different photomagnetic behaviors for the high field magnetization and coercive fields with energy scales of 25 K and 200 K, respectively. Importantly, the magnitude of the light-induced change in the magnetization is found to be specific to the synthesis protocol, with aggregated nanoparticles showing a larger effect than isolated particles. Mössbauer spectroscopy provides additional evidence of the differences between the aggregated and isolated nanoparticle samples. For $T \lesssim 25$ K, the photo-response arises from magnetic disorder generated by an elevated electronic temperature in the surface layer of the particles, thereby leading to a decrease in magnetic volume. For 25 K $\lesssim T \lesssim 200$ K, the electronic and phononic reservoirs are more intimately coupled, so the photo-induced magnetic response follows the temperature dependence of the magneto-crystalline anisotropy. A similar response in manganese ferrite suggests that the mechanism is general. *Published by AIP Publishing.*
https://doi.org/10.1063/1.5040327

I. INTRODUCTION

Optically switchable magnets are an important class of functional materials having potential applications in magneto-optical and optoelectronic devices.[1–3] The interplay of light and magnetism to control properties offers routes to novel technologies such as energy assisted magnetic recording, which can increase the areal density of information storage by orders of magnitude.[4] Traditional magnetic solids and films of oxides, metals, and metal alloys have been shown to switch magnetically with light on femtosecond to picosecond timescales,[5–8] while the lifetime of the resulting change in magnetism depends on the composition and geometry of the samples and the helicity of the light being employed.[9–11] Alternatively, certain molecule-based materials such as Prussian blue analogues, spin crossover compounds, and their heterostructures show persistent photo-induced magnetism,[12–15] and recent experiments have elucidated the aspects of the switching timescales and lifetimes as a function of the sample composition and morphology.[16,17] Light-controllable coercivity in Fe:Au alloy nanostructures[18] and light-induced magnetization changes in Fe nanoparticles coated with the photochromic azobenzene ligand[19] are further intriguing

examples promoting ideas for next generation spintronic and or photonic devices.

There have been some important observations of photo-induced magnetism in doped spinel ferrites, such as Al-substituted Fe_3O_4 and Zn- or Ti-substituted $NiFe_2O_4$ cluster glass thin films.[20,21] Upon irradiation, inter-valence charge transfer (IVCT) leads to melting of the cluster glass state and spin realignment, giving rise to an increase in magnetization. Additionally, $(Mn, Zn, Fe)_3O_4$ nanocrystalline films have shown a light-induced increase in magnetization at room temperature with X-ray magnetic circular dichroism, giving evidence for IVCT, leading to changes in the magnetic anisotropy.[22]

The current study reinvestigates the light-induced coercivity changes, $\Delta H_c \sim 3$ kOe at 10 K, in cobalt ferrite $(CoFe_2O_4)$ nanoparticles first reported by Giri *et al*.[23,24] and extends these initial reports. In line with related systems, optical electron transfer between Co^{2+} and Fe^{3+} ions to generate Co^{3+} and Fe^{2+} with reduced anisotropy was proposed to explain the light-induced changes in cobalt ferrite.[23,24] The net magnetic moment is conserved during such a process, which was consistent with the authors' report of no change in remanent and saturation magnetization. The 170 K upper limit for the light induced changes in coercivity was attributed at the time to a metal-insulator transition.

Motivated by renewed interest in these topics, the work reported herein presents a more comprehensive set of

a)T. V. Brinzari and D. Rajan contributed equally to this work.
b)Electronic mail: meisel@phys.ufl.edu
c)Electronic mail: talham@chem.ufl.edu

analyses of the photomagnetic effects in cobalt ferrite nanoparticles. In addition to the light-induced coercivity changes communicated by Giri *et al.*,[23,24] we observed changes in the remanent magnetization (M_{rem}) and the magnetization in 70 kOe (M_{70kOe}) upon irradiation with light. Further experimental evidence suggests that the mechanism of the effect goes beyond an optically triggered charge transfer. The photo-effects are found to depend on the specific synthesis protocol of the sample with aggregates of nanoparticles formed by coprecipitation, showing a significantly larger effect than isolated nanoparticles formed by thermal decomposition. Field and temperature dependent magnetometry data implicate the interaction of light with spins at the surface of the particles as a likely origin of the novel behavior. Specifically, for temperatures $T \lesssim 25\,K$, irradiation raises the electronic temperature of the surface layer above the equilibrium lattice (phonon) temperature. This type of effect is commonly known to onset at a crossover temperature $T^* \approx c\hbar/(k_B L)$, where c is the speed of sound and L is the characteristic length scale of the system.[25] For $c \sim 3.5\,km/s$ and $L \sim 7\,nm$, $T^* \sim 25\,K$. Consequently for $T \lesssim T^*$, irradiation induces magnetic disorder in the surface layer, and the effective magnetic volume is decreased, most notably leading to the decrease in the coercive field. Since $T \geq 2\,K$ in this work, the electronic temperature quickly[26] relaxes back to the phonon temperatures when the heat source (light) is switched off.[27] For $25\,K \lesssim T \lesssim 200\,K$, the electronic reservoir is in intimate contact with the phonon one, so the overall photo-induced magnetic response is governed by the bulk magneto-crystalline effects.

II. EXPERIMENTAL METHODS

A. Synthesis and characterization

Cobalt ferrite nanoparticles were synthesized using both coprecipitation and thermal decomposition syntheses as described in the literature,[28–30] and a variety of methods were used to characterize their compositions. Specifically, inductively coupled plasma atomic emission spectroscopy (ICP-AES) was used to determine the Co:Fe ratios and were recorded on a Perkin-Elmer Optima 3200 instrument. Powder X-ray diffraction (XRD) patterns were collected on a PANalytical X'Pert Powder diffractometer with a Cu source in the 2Θ range of $15°-80°$ and with a step size of $0.008356°$. The diffraction patterns were indexed to a spinel ferrite phase, Fd-3m (JCPDS PDF No. 221086). Transmission electron microscopy (TEM) was performed with a JEOL-2010 transmission electron microscope operating at $200\,kV$. The TEM samples were prepared by dispersing 1 mg of sample in 1 ml solvent, water or hexane, by sonication and drop casting $40\,\mu l$ of solution on the grid (carbon film on a holey carbon support film, 400 mesh, copper from TED-Pella, Inc.). The recorded micrographs were analyzed using ImageJ software.[31] The mean diameters and size distribution of each sample were obtained from a statistical analysis of particles from different regions of the grid.

1. Coprecipitation method, samples 1 and 1a

For sample **1**, cobalt chloride, $CoCl_2 \cdot 6H_2O$ (5 mmol), and ferric chloride, $FeCl_3 \cdot 6H_2O$ (10 mmol), were dissolved in 50 ml of water. This solution was added dropwise using an addition funnel to a solution of NaOH (0.375 mol) in 100 ml water. After complete addition, the mixture was heated at $90°C$ for 1.5 h. The black precipitate was washed with deionized water and acetone, and the resulting black powder was annealed in air inside an oven at $260°C$ for 24 h. For sample **1a**, the same procedure was used, except that the NaOH solution was 0.15 mol in 100 ml water. ICP-AES data: Sample **1** (Co:Fe) = 1.00:(2.07 ± 0.04). Sample **1a** (Co:Fe) = 1.00:(2.00 ± 0.03). The spinel ferrite unit cell constant was calculated from the peak position of the most intense reflection (311) to be 8.335 Å. Both samples were aggregates of smaller particles. The intra-aggregate particle size assessed using TEM was $7 ± 2\,nm$ for sample **1** and $17 ± 5\,nm$ for sample **1a**. Further characterization details for all samples appear in Table I and in the supplementary material (Figs. SM1–SM13 and Tables SM1–SM3).

2. Thermal decomposition method, samples 2, 2a, and 2b

A mixture of phenyl ether (10 ml), oleic acid (2.5 ml), and oleylamine (2.5 ml) was degassed for 30 min followed by addition of $Co(acac)_2$ (0.5 mmol) and 1,2 hexadecanediol (5 mmol). This mixture was heated to $140°C$ before a solution of $Fe(acac)_3$ (1 mmol) dissolved in 5 ml phenyl ether was added drop wise. The resulting solution was then heated to $260°C$ and refluxed for 3 h. After cooling to room temperature, the reaction mixture was washed and centrifuged with ethanol and acetone to obtain a black powder upon drying. Samples **2** and **2a** were each prepared in this way and are two different batches using the same protocol. Sample **2b** was obtained by annealing part of sample **2** in air at $260°C$ for 24 h. ICP-AES data: sample **2** (Co:Fe) = 1.00:(1.96 ± 0.04) and sample **2a** (Co:Fe) = 1.00:(1.92 ± 0.03). X-ray diffraction confirms the spinel ferrite phase, Fd-3m (JCPDS PDF No. 221086). Unit cell constants for samples **2** and **2a** are 8.380 Å and 8.393 Å, respectively.

B. Magnetometry

The dc magnetic properties were investigated using a commercial superconducting quantum interference device (SQUID) magnetometer (Quantum Design MPMS-XL7). The optical measurements were performed with a homemade quartz optic sample rod attached to a tungsten halogen lamp via a fiber optic patch cable, with a nominal transmission window in the range of 400 nm to 2200 nm. Wavelength dependent measurements were performed using several high-power LED sources (Thorlabs) with discrete wavelengths in the range from 405 nm to 850 nm. The power at the sample was calibrated outside the magnetometer. For broadband illumination, the power was approximately 4 mW. For the LEDs, the power was set to 1.5 mW or was at the levels indicated in the text. The samples were prepared by dispersing the cobalt ferrite nanoparticles (1% by weight)

TABLE I. Summary of the nomenclature of the samples and their associated synthesis protocols, forms, mesoscale (aggregate) and nanoscale (nanoparticle) sizes, the percentage of ion compositions on the two crystallographic sites (O_h and T_d) as determined by analyses of XPS and Mössbauer data, and the photo-induced changes of the coercive field (H_c), remanent magnetization (M_{rem}), and the magnetization value at 70 kOe (M_{70kOe}). The uncertainty in the percentage of distribution of the ions as determined by XPS was approximately 10% for both samples studied. The occupancy values, obtained from the Mössbauer data, were derived from a deconvolution of the field dependent spectra recorded at 4.2 K while assuming that the major and minor spectral components occupy the O_h and T_d sites, respectively, as discussed in Secs. II D and SM3. Copt = coprecipitation, TD = thermal decomposition, and PA = post-annealed.

Sample ID	Synthesis Protocol	Overall Form	Mesoscale Size (nm)	Nanoscale Size (nm)	XPS					Mössbauer[a]		Photo–induced changes[b]		
												(Dark–light)/(dark) (%)		
					Co^{2+} (O_h)	Co^{2+} (T_d)	Co^{3+} (O_h)	Fe^{3+} (O_h)	Fe^{3+} (T_d)	Fe^{3+} (O_h)	Fe^{3+} (T_d)	ΔH_c	ΔM_{rem}	ΔM_{70kOe}
1	Copt	Aggregate	270 ± 90	7 ± 2	...	...	...	...	...	...	...	21	10	7
1a	Copt	Aggregate	265 ± 90	17 ± 5	43	34	23	66	34	56 ±2	32 ± 3	23	6	12
2	TD	Isolated	...	6 ± 1	...	...	...	...	...	...	...	8	9	4
2a	TD	Isolated	...	4 ±1	60	28	11	61	39	56 ±2	32 ± 3	13	7	7
2b	TD-(PA)	Aggregate	300 ± 80	6 ± 1	...	...	...	...	...	...	...	6	2	6

[a]Approximately 10% of the Mössbauer intensity is not assignable, as detailed in supplementary material.
[b]At $T = 10$ K.

in an optical grade epoxy (Stycast 1266 from Emerson & Cuming) cured at room temperature and then trimming the resulting piece to achieve a disc-shaped sample with nominal dimensions 0.24 cm × 0.13 cm (diameter × height). As an alternative approach, nanoparticles were also spread as a thin layer between two pieces of transparent tape. However, due to the high absorption of cobalt ferrite, the amount of material strongly influences the magnitude of the photomagnetic effect. The dilution of cobalt ferrite is a *critical step* in the investigation of its photomagnetic properties, so samples mixed with epoxy were used in this work. The magnetization versus field/temperature dependences in the "dark state" were measured after field cooling the sample in 0.1 kOe from room temperature. Irradiation experiments at a specific temperature were performed in a field of 0.1 kOe after field cooling the sample from room temperature. Unless otherwise noted in the text, the "light state" was established by irradiation after the magnetic response was saturated with respect to time, and subsequently, the magnetization in the light state was measured while maintaining the irradiation. The ac measurements were performed on a second commercial magnetometer (Quantum Design MPMS-5S).

C. X-ray photoelectron spectroscopy

X-ray photoelectron spectroscopy measurements were collected on a ULVAC-Phi X-ray photoelectron spectroscope (XPS) from Physical Electronics with a Mg K_α X-ray source (1253.6 eV). Data were plotted and fit using Phi Multipak v. 9.3 XPS software. The sample powder was spread on a piece of transparent tape having dimensions of 10 mm × 10 mm. The instrument utilizes a shower head irradiation style, and X-rays covered the entire sample area. Survey spectra were collected at 10 sweeps over a binding energy range of 0 to 1000 eV with a step size of 0.5 eV/step and a pass energy of 89.45 eV. The sample tilt was set to 45°. High resolution data were collected over a range that includes the carbon 1s and the main lines for elements of interest, with a step size of 0.1 eV/step and a pass energy of 35.7 eV. The sample tilt was again set to 45°. Multiplex data

typically included 10 to 40 scans per peak in order to achieve a reasonable signal to noise ratio.

D. ^{57}Fe Mössbauer spectroscopy

Field and temperature dependent ^{57}Fe Mössbauer spectra were recorded using a spectrometer fitted with a Janis 8DT Super Varitemp flow-type cryostat. The cryostat was cooled with liquid helium and was equipped with an 80 kOe American Magnetics superconducting magnet. When a 100 W Na-lamp was used to irradiate the sample, a liquid helium-cooled cryostat, equipped with optical windows but without a magnet, was used to measure zero-field spectra at 4.2 K. For both cryogenic configurations, the spectrometer was operated in a constant acceleration mode. The source consisted of 100 mCi ^{57}Co dispersed in a Rh metal foil. The external field was applied parallel to the propagation direction of the incident γ-radiation. The samples were obtained by dispersing 10 mg to 15 mg cobalt ferrite nanoparticles as neat powder in about 0.2 ml of mineral oil and were contained in custom made Delrin® or polyethylene containers. Isomer shifts are reported with respect to the centroid of a room temperature spectrum recorded for a standard α-Fe metal foil. The experimental spectra were analyzed using the WMOSS software [SEE Co. (formerly Web Research Co.), Edina, MN] and the Voigt-based model first described by Rancourt and Ping.[32] This approach allows for the description of an arbitrary hyperfine field distribution (HFD) in terms of a discrete sum of individual Gaussian components. Each Gaussian component can be understood as originating from a large sum of elemental spectra with intensities that follow Gaussian distributions and differ from one another in the values of a particular parameter. Furthermore, each Gaussian component is defined by three parameters, namely, p[%], a weight factor which, assuming identical f-recoilless fractions, represents the fraction of the total iron amount that is accounted for by the respective component, and H_{obs} [kOe] and dH[kOe], which account for the centroid and the width of the Gaussian HFD. In zero-field, H_{obs} [kOe] denotes the H_0 of the respective component. Several additional parameters are used to describe the elemental sextet spectra

comprising the HFD: Γ, the full width at half maximum (FWHM) of the intrinsic Lorentzian line shape; δ, the isomer shift; ϵ, the electric field gradient (EFG) tensor component along the internal field; and h_1/h_3 and h_2/h_3, the height ratios of the outer (1, 6) lines to the inner (3, 4) lines and of the middle (2, 5) lines to the inner (3, 4) lines, respectively.

III. RESULTS

A. Light-induced changes in coercivity

The cobalt ferrite samples discussed in this work (Table I) were prepared by two different synthesis protocols, the coprecipitation[28] (Copt) procedure yielding aggregates of nanoparticles, samples **1** and **1a**, and the thermal decomposition[29,30] (TD) process giving isolated nanoparticles, samples **2** and **2a**. The coprecipitation batches are composed of aggregates of an average size of 270 ± 90 nm for **1** and 265 ± 90 nm for **1a**. For **1**, the nanoparticles within the aggregates have sizes of 7 ± 2 nm, whereas the nanoparticles in **1a** are slightly larger with nominal sizes of 17 ± 5 nm. On the other hand, two batches of monodispersed isolated nanoparticles with an average diameter of 6 ± 1 nm for **2** and 4 ± 1 nm for **2a** are formed using the thermal decomposition protocol, which isolates particles as a result of a residual organic coating. Typical TEM images for each sample are shown in insets of Fig. 1, and plots of the size distributions for each sample are given in Figs. SM1–SM4.

Elemental composition data from ICP-AES indicate that samples **1**, **1a**, **2**, and **2a** have similar chemical compositions. X-ray photoelectron (XPS) and Mössbauer spectroscopies were used to determine the site occupancies (O_h and T_d) of the metal ions for **1a** and **2a**. These data indicate that the two different synthesis protocols give similar metal ion site occupancies and chemical composition (Table I). A detailed description of the XPS and Mössbauer data sets and analyses can be found in Figs. SM5–SM8, Tables SM2 and SM3, and the associated text.

Changes in coercivity with light, as first reported by Giri *et al.*,[23,24] whose results have not been the subject of any further work reported in the literature up to the findings reported herein, were observed for both coprecipitation samples (Fig. 1). The 10 K dark state coercivity of sample **1** is 14.98 ± 0.01 kOe and of sample **1a** is 13.93 ± 0.03 kOe. Irradiation with broadband light leads to a decrease in the coercivity of both samples, specifically $\Delta H_c = H_c^{dark} - H_c^{light} = 3.09 \pm 0.05$ kOe for **1** and $\Delta H_c = 3.19 \pm 0.06$ kOe for **1a**. No significant difference in the photomagnetic response of the two batches was observed in this investigation. Sample **2**, prepared by thermal decomposition, displays a narrower hysteresis loop with a coercivity of $H_c = 7.24 \pm 0.04$ kOe, and this smaller coercivity is due to separation of the magnetic nanoparticles achieved by the surfactant coating. Additionally, the high field magnetization value $M_{70kOe}^{dark} = 73.72$ emu/g is higher than the corresponding values for **1** and **1a**, which are 60.90 emu/g and 62.45 emu/g, respectively. Different values of M_{70kOe} for samples **1**, **1b**, and **2**, as well as the apparent absence of saturation at 70 kOe, are typical responses when considering variations of sample synthesis and resulting morphology.[33] Upon annealing sample **2** in air
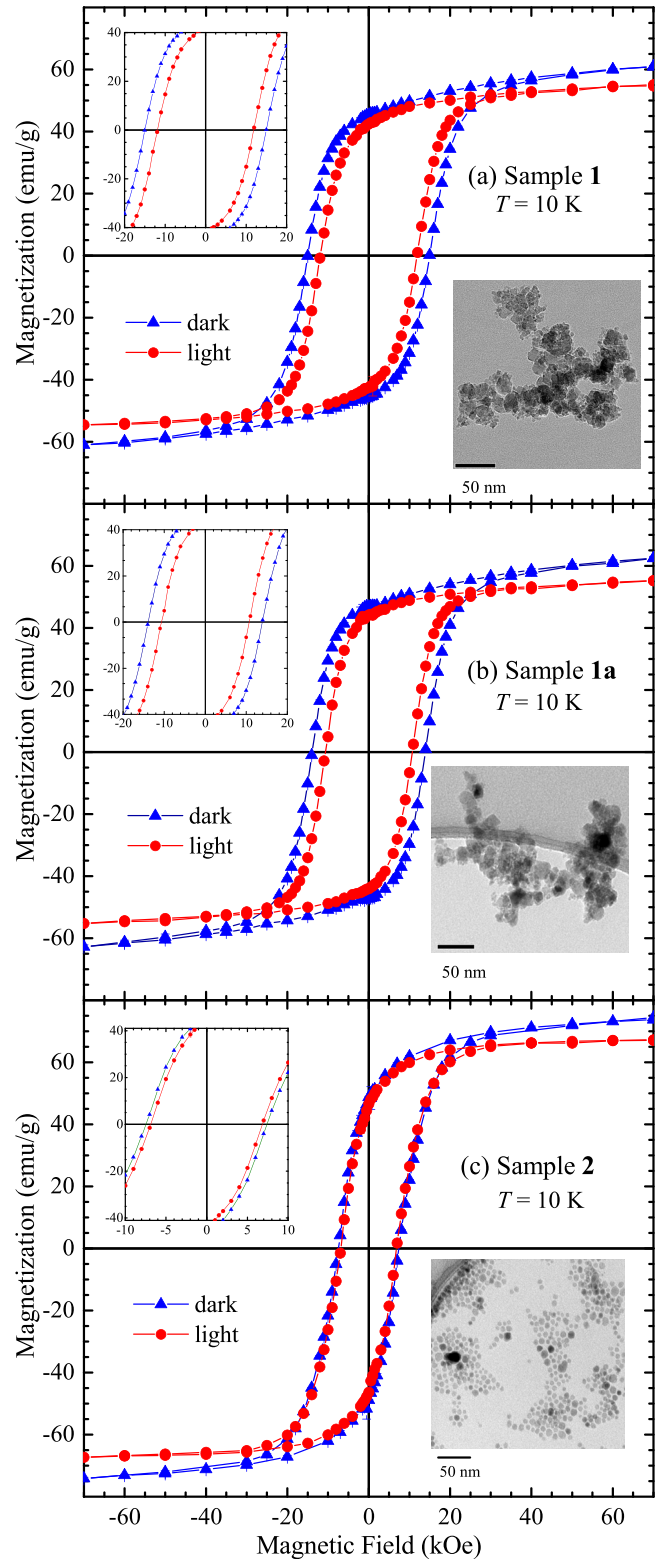

FIG. 1. Magnetization versus applied magnetic fields as measured in the dark and light states at 10 K for (a) sample **1**, (b) sample **1a**, and (c) sample **2**. Insets at the top left of each panel provide an expanded view of the low field regions and those at the bottom right are the TEM micrographs of the respective samples.

for 24 h at 260 °C to obtain sample **2b**, the isolated particles aggregate, and the coercivity was modified to a value of 12.31 ± 0.01 kOe, indicating an increase in the effective size of the magnetic domains in the aggregated sample. Upon

irradiation of **2** with broadband light, the coercivity change was $\Delta H_c = 0.58 \pm 0.06$ kOe, whereas after annealing to become sample **2b**, a small enhancement of the light-induced change was observed as $\Delta H_c = 0.78 \pm 0.02$ kOe. The samples evaluated in this study do not show the previously reported[23,24] particle size dependence on the light-induced change in coercivity, but the influences of aggregation may mask any particle size dependence. Overall, the light-induced changes in magnetic coercivity of cobalt ferrite nanoparticles, originally reported by Giri *et al.*,[23,24] are generally reproduced.

B. Temperature dependences of the light-induced changes in coercivity and remanent magnetization

The magnitude of the light induced-change in coercivity was previously reported to become smaller with increased temperature, tending to zero near 170 K.[24] The present study confirms this gradual decrease in the magnitude of the light-induced coercivity change as the temperature is increased [Fig. 2(a)]. Interestingly, these thermal trends can be compared to the behavior of the samples in their dark states [Fig. 2(b)]. Clearly, the temperature dependence of the light-induced coercivity change closely resembles the temperature trend of the coercive field in the dark state, which displays a constant drop up to ≈ 200 K, followed by a change in the slope and slower decrease up to 300 K. In addition to the reduced coercivity during irradiation, changes in the remanent magnetization are also observed [Fig. 2(c)]. Indeed, the temperature dependence of the light-induced remanent magnetization (ΔM_{rem}) mimics the same thermal trend observed for the coercivity as ΔM_{rem} decreases up to 200 K.

As potential explanation for the disappearance of the photo-induced changes near 170 K, Giri *et al.*[24] suggested the possibility of a metal-insulator transition analogous to the Verwey transition in magnetite (Fe_3O_4).[34] More specifically, Giri *et al.*[24] suggested that, below 170 K, the absorption of a photon leads to a $Co^{2+} \rightarrow Fe^{3+}$ electron transfer, thereby providing a localized charge and a reduction in the coercivity. Above 170 K, they argued that a rapid charge exchange results in a fast relaxation of the light-induced state, so no significant magnetic changes were detected. Indeed, Fe_3O_4 is known to possess a crystallographic distortion and abrupt changes to its electrical conductivity, magnetic susceptibility, and specific heat at its Verwey transition.[35–41] To explore this hypothesis, we looked for structural or magnetic anomalies associated with the disappearance of the photo-effects near 200 K. An X-ray diffraction study on **1a** (Fig. SM9) reveals no signatures of a structural transition (or symmetry breakdown) from 300 K down to 100 K. Moreover, the temperature dependent magnetization displays no discontinuities or changes in behavior near or at 200 K (Fig. SM10). Although a direct measurement of the electrical properties is necessary to verify the metal-insulator transition, if it is present, our structural and magnetic data demonstrate that the nature of the transformation is clearly different from the Verwey transition in magnetite.

Proximity to a magnetic blocking temperature (T_B) could be another explanation for the disappearance of the light-induced changes in coercivity. However, dc
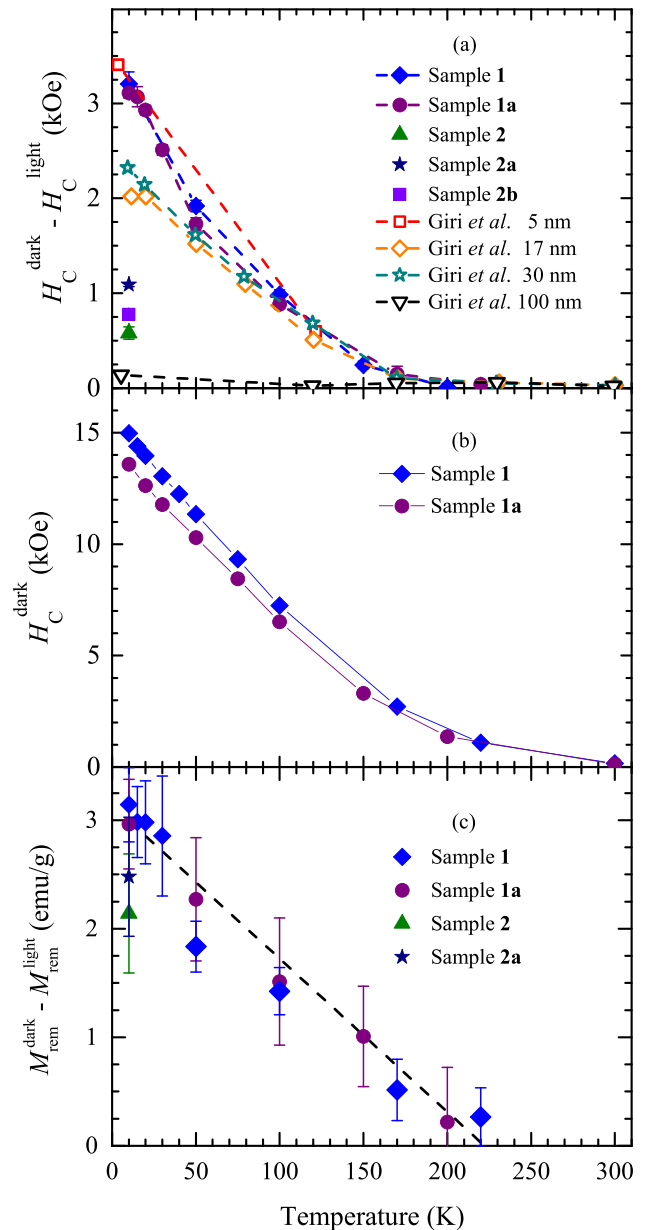

FIG. 2. (a) Temperature dependences of the light-induced coercivity change for cobalt ferrite samples studied in this work and those reported by Giri *et al.*[23,24] (b) Temperature dependences of the coercivity without irradiation (dark state). (c) Temperature dependences of the light-induced change in the remanent magnetization for cobalt ferrite samples studied in this work. In all panels, the lines are guides for the eyes.

magnetization measurements (Fig. SM10) and the Mössbauer analysis, *vide infra*, indicate that the coprecipitated samples remain blocked to 300 K. On the other hand, ac measurements of the zero-field cooled magnetization at frequencies of 10 Hz, 100 Hz, and 1 kHz (Fig. SM11) show small peaks, hinting that a fraction of the particles might experience lower blocking temperatures, between 200 K and 250 K, perhaps contributing to the disappearance of the light-induced effects near those temperatures. Nevertheless, the change in coercivity shown in Fig. 2(a) clearly follows the temperature profile of the dark state coercivity [Fig. 2(b)], suggesting that the changes with temperature have a similar origin.

C. Wavelength and power dependences of the light-induced coercivity changes

In the report by Giri *et al.*,[24] the light-induced changes were associated with a $Co^{2+} \rightarrow Fe^{3+}$ charge transfer initiated by optical absorption near 2 eV. In order to test this assertion, the wavelength-dependent responses within the visible spectrum were probed by using a series of LED sources. The light-induced changes in the coercivity for samples **1** and **1a** as a function of the wavelength (and energy) of the excitation source are shown in Fig. 3. The absence of a maximum near 2 eV indicates that the excitation driving the effect is broad in nature and cannot be attributed solely to the Co^{2+}/Fe^{3+} electron transfer transition centered at 2 eV.[42,43]

On the other hand, the broad nature of the excitation energy response correlates well with the superposition of two aspects of the interaction of light with the nanoparticles, namely, optical absorption and skin depth. Specifically, the optical absorption spectrum of a thin film of cobalt ferrite shows broad absorption in the 1.2 eV to 6 eV range with an indirect bandgap at 1.2 eV,[44] and it is important to recall that finite length scale effects can cause the optical absorption of nanoparticles to be different from the bulk.[45,46] Nevertheless, the overall absorption is higher at 400 nm and falls off to lower values with the increasing wavelength. Contrastingly, the skin depth value is about 1.1 nm at 400 nm and increases smoothly with the increasing wavelength to nominally 1.6 nm near 850 nm.[47] The opposing wavelength dependences of the absorption and skin depth generate the overall trend shown in Fig. 3. In other words at lower wavelengths, the two effects play a combined role in influencing the (dark–light) changes of the coercive field, whereas for $\lambda \gtrsim 700$ nm, the optical absorption grows increasingly weaker, so the trend is softer in this regime where the skin depth effect remains intact. Furthermore, additional studies were performed with the infrared radiation $\lambda \gtrsim 700$ nm filtered from the broadband light source, and consistent with the aforementioned interplay
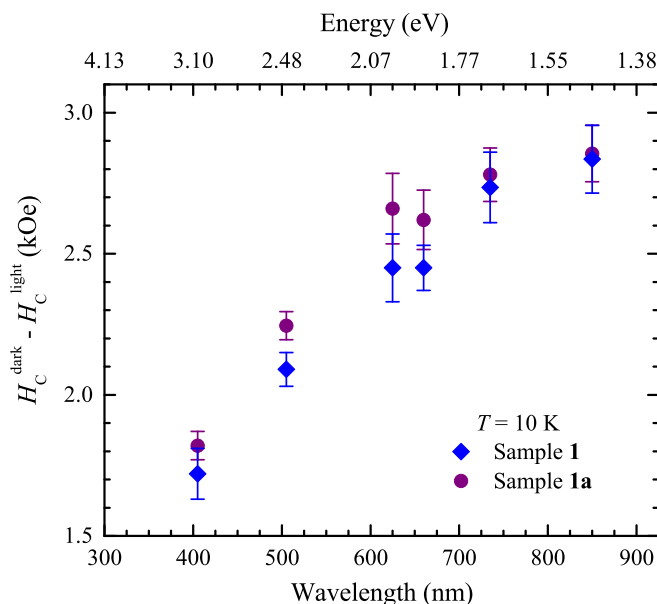
between the absorption and skin depth, no substantial variations of the light-induced changes in coercivity were observed when compared to the unfiltered results.

Finally, in order to differentiate lattice thermal effects from the photo-induced changes to the electronic reservoir, the power response from two wavelengths was mapped at 10 K (Fig. SM12). In addition, on/off switching profiles at 10 K indicate that the response to irradiation is significantly faster than the measurement time and the overall dark state magnetism is stable over hundreds of minutes (Fig. SM13). Altogether, these results indicate that macroscopic lattice heating is not the source of the light-induced changes of the magnetic response, and instead, the dramatic changes detected below nominally 25 K arise from an effective heating of the electronic reservoir near the surface.

D. Light-induced change in magnetization at 70 kOe

For each magnetic field, the isothermal ($T = 10$ K) magnetization value of the light state is less than the corresponding response of the dark state (Fig. 1). In fact, the $M(H \gtrsim 30)$ kOe response is noticeably different, as the irradiated samples have weaker slopes than their dark state counterparts. In fact, a lowering of high field $M(H)$ values has been ascribed to increased surface spin disorder as the nanoparticle size decreases.[50] Consequently, the temperature dependences of the M_{70kOe} values were measured for both the aggregated and isolated particle samples.

As shown in Fig. 4, dramatic changes in M_{70kOe} are detected with irradiation at low temperature, and these changes dissipate as the temperature is raised above 25 K. It is important to note that the value of the low-temperature, optically quenched, high-field magnetization of sample **1a** is substantially smaller than the room temperature value [Fig. 4(a)], which again indicates that macroscopic *lattice* heating is not the source of the light-induced effects. This interpretation is supported by the rapid switching between the magnetic states when the irradiation is toggled on and off [Fig. SM13]. Furthermore, characterization of our homemade optical probes indicates that similar samples experience thermal changes of less than 1 K when $T < 50$ K.[51]

A similar effect is observed for the isolated particles in sample **2**, although the magnitude is comparatively smaller [Fig. 4(b)]. The differences in the dark and light state magnetization at 70 kOe as a function of temperature for the aggregated samples are shown in Fig. 5(a). Furthermore, varying the power of the irradiation source for the aggregated samples showed a linear dependence with increasing power, and wavelength dependent studies showed an overall decrease in ΔM_{70kOe} at longer wavelengths [Figs. 5(b) and 5(c)]. Importantly, this behavior is distinct to the high field magnetization and is opposite to the trends observed for the coercivity (Fig. 3). These differing trends indicate the presence of two energy scales, one at approximately 25 K and the other near 200 K, hinting at the possibility of more than one underlying mechanism for the photo-induced magnetization changes in cobalt ferrite nanoparticles.

FIG. 3. Light-induced changes in coercivity $H_c^{dark} - H_c^{light}$ as a function of the wavelength (and energy) of the excitation source.
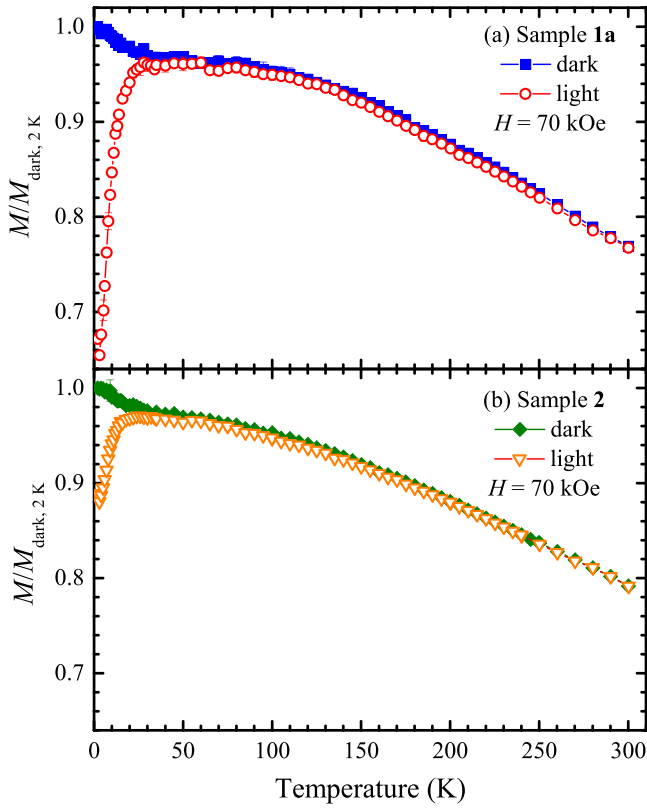
FIG. 4. Temperature dependences of the dark and light magnetization values at 70 kOe, normalized to the dark state value at 2 K, for (a) sample **1a** and (b) sample **2**. In (a), it is noteworthy that, with irradiation, the values at the lowest temperatures are less than the value at 300 K.

E. Field and temperature dependences of Mössbauer spectra

The dynamics of the magnetic properties of samples from each type of synthesis protocol were investigated using ^{57}Fe Mössbauer spectroscopy (see Sec. II D). Since both samples were found to have similar chemical compositions but distinctly different morphologies, where sample **1a** is composed of aggregates of nanoparticles and sample **2a** consists of isolated nanoparticles (Table I), this study assesses the influence of aggregation on the spectroscopic behavior. The datasets and their analysis will be introduced first, contrasting the similarities and differences of the overall responses. Next, a standard domain-lattice description to extract dynamical information is presented followed by attempts to resolve the contributions into bulk and surface components.

While the field-dependent spectra recorded at 4.2 K are essentially identical for both samples (Figs. 6 and SM7), the temperature dependences of the spectra are significantly different (Figs. 7 and SM8). As the temperature is increased above 50 K, the zero-field spectra recorded for sample **2a** reveal a superposition of doublet and sextet components. At 250 K, the doublet component accounts for nearly half of the spectral area and is characterized by an isomer shift $\delta = 0.36(2)$ mm/s, quadrupole splitting $\Delta E_Q = 0.72(5)$ mm/s, and a rather broad linewidth $\Gamma = 0.7$ mm/s. In contrast, regardless of the temperature, no doublet component was observed for sample **1a** (Fig. SM8). Finally, zero-field
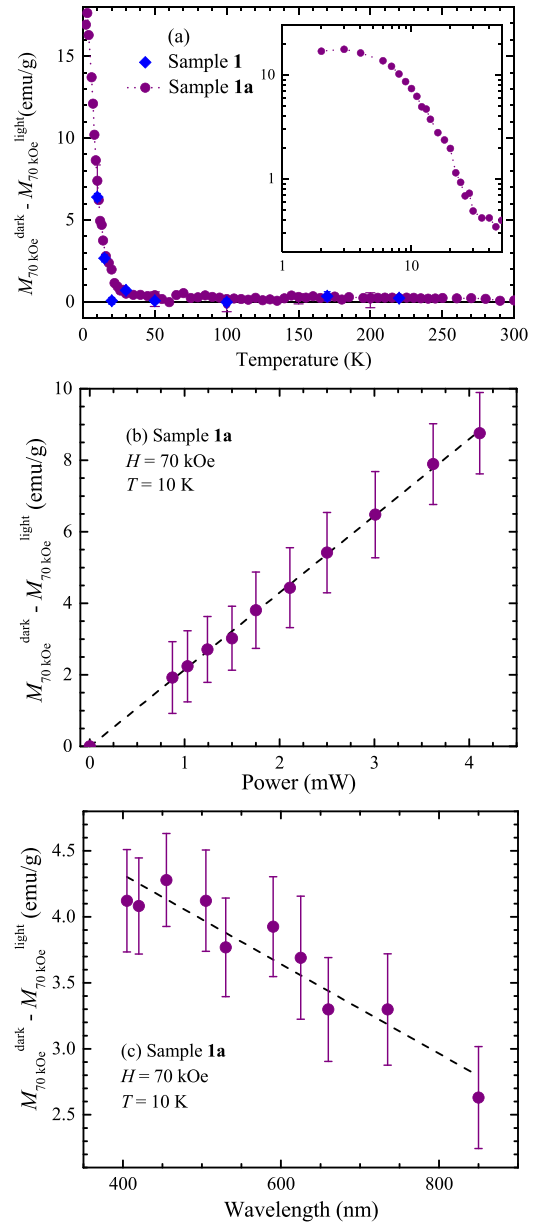

FIG. 5. Light induced changes of the magnetization at 70 kOe as a function of (a) temperature with white light irradiation at a constant power of 4 mW, (b) power of white light irradiation, and (c) wavelength at a constant power of 1.5 mW. In (a), the data for sample **1a** are from Fig. 4(a). A few illustrative data points for sample **1** are shown, and the uncertainty is typically less than the size of the symbols. The inset shows a log-log plot for sample **1a** below 50 K.

spectra were collected at 4.2 K while irradiating the samples with white light. However, within the uncertainty of the measurements, no light-induced changes in the internal fields were observed.

In zero-field, the magnetic energy (E) of a classical magnetic particle or domain is given by

$$E = KV \sin^2\theta, \tag{1}$$

where K is the magnetocrystalline anisotropy constant, V is the volume of the nanoparticle, and θ is the angle between the magnetic moment of the particle and its anisotropy axis.[52,53] So, E possesses a maximum ($\theta = \pi/2$) and two
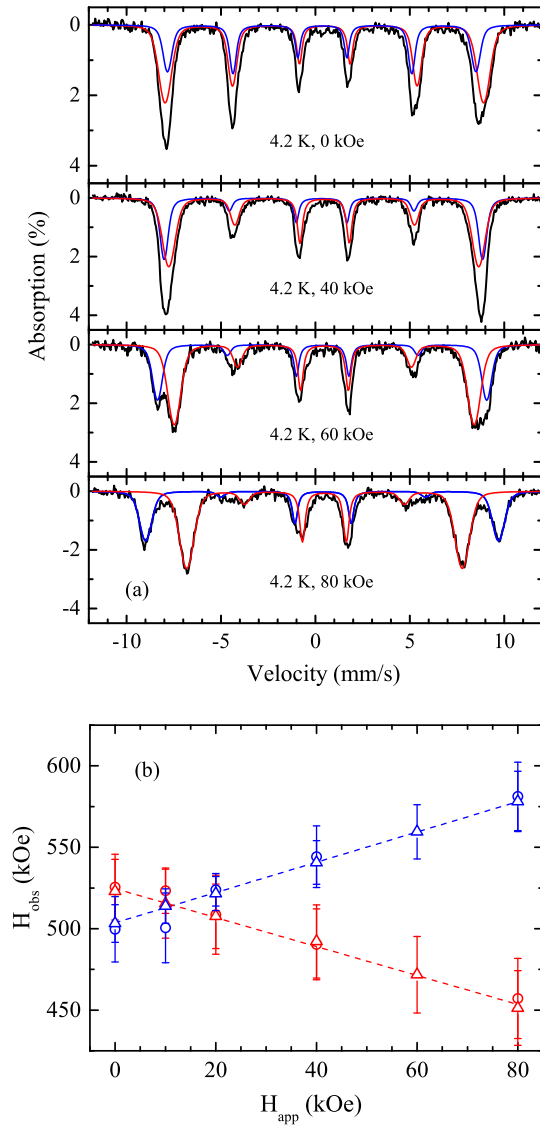
FIG. 6. (a) Field-dependent ^{57}Fe Mössbauer spectra recorded for sample **1a** at 4.2 K. The spectra were deconvoluted into two components, shown in red and blue, which are associated with a ferrimagnetic ordered state. (b) Field-dependence of the observed hyperfine-splitting, H_{obs}, for each component at 4.2 K for sample **1a** ($\triangle$) and sample **2a** ($\bigcirc$) as a function of the applied magnetic field, H_{app}. The error bars correspond to the FWHM of the Gaussian distributions used to determine the H_{obs} values. The hyperfine splitting parameters derived from the fitting of the 4.2 K, 80 kOe spectra are given in Table SM3.

minima ($\theta = 0$, π), and the height of the energy barrier is given by KV. At low temperature, the magnetization vector is essentially aligned with the anisotropy axis. Increasing the temperature such that $k_B T \geq KV$ leads to fluctuations of the magnetization between the two orientations. At low temperatures, the fluctuation rate of the magnetization vector associated with the ^{57}Fe nuclei is typically small with respect to rate of the nuclear Larmor precession, 4×10^{10} s^{-1}.[54] Consequently, the ^{57}Fe nuclei experience an effective field, which in turn leads to the observation of a magnetic hyperfine splitting pattern, giving a sextet spectrum. Alternatively, if the lifetime of the magnetization in a given state is shorter than the Mössbauer measuring time $\tau_M \sim 10^{-8}$ s, the magnetic hyperfine interactions are averaged and only a
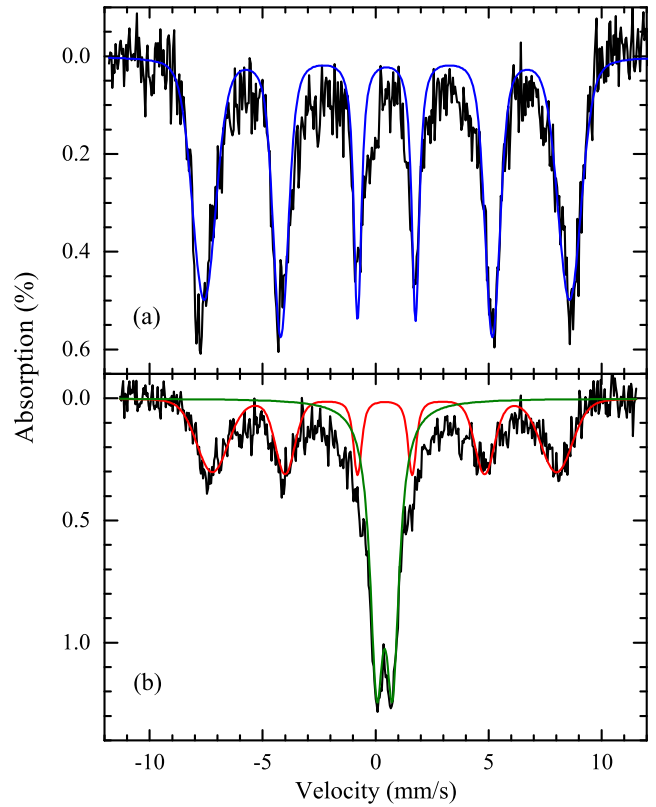

FIG. 7. The ^{57}Fe Mössbauer spectra recorded at 250 K in zero applied field for (a) sample **1a** and (b) sample **2a**. Whereas the spectra for **1a** are similar at 4.2 K and 250 K, the data for **2a** indicate sextet nature at 4.2 K, with a doublet contribution as the temperature is increased above 90 K (Fig. SM8). In (b), the spectrum of **2a** is deconvoluted into a doublet (green line) and sextet (red line) with nearly equal spectral areas.

quadrupole doublet is observed. For a given nanoparticle, the average time between two magnetization flips, τ, is given by the Néel-Brown expression

$$\tau = \tau_o \exp(k_B T / KV), \tag{2}$$

where τ_o is a time constant.[55] Typically, a collection of nanoparticles exhibits a distribution in particle sizes which leads to a distribution in relaxation rates. In the case where $\tau \approx \tau_M$ for magnetically isolated particles, the distribution in particle sizes leads to spectra consisting of a superposition of doublet and sextet components. The temperature at which the two components have equal areas is defined as the Mössbauer blocking temperature, T_{MB}, and can be related to the superparamagnetic relaxation rate as[56]

$$T_{MB} = \frac{KV}{k_B \ln(\tau_M/\tau_o)}. \tag{3}$$

Inspection of Fig. 7 reveals that for sample **2a**, $T_{MB} \approx 250$ K. In the case of **1a**, the failure to observe a quadrupole doublet, even at 250 K, can be traced to the presence of significant long-range dipole interactions which, in a first approximation, can be considered to lead to an increase in the energy barrier between the two minima and thus to an increase in the relaxation time.[57,58] Consistent with this observation, no blocking temperature was observed for this sample up to 300 K by SQUID magnetometry. Together, the

Mössbauer spectroscopy and SQUID magnetometry studies show that the effects of the inter-particle interactions present in sample **1a**, which is composed of aggregates of nanoparticles, are relatively absent in **2a**, which consists of isolated nanoparticles.

Interestingly, the dark state magnetization at 70 kOe does not saturate even at 2 K, for either the aggregated particle sample **1a** or the isolated particle sample **2a** (Fig. 4). A pronounced upturn in the high-field magnetization is observed below 25 K, which is also the same temperature below which demagnetization in the light state is observed. This steep rise in high field magnetization below 25 K has been previously observed in cobalt ferrite nanoparticles and attributed to surface spin disorder.[59,60] The physical origin of this behavior can be explained by a core-shell model, with a ferrimagnetically ordered core and a magnetically inert shell resulting from broken symmetry and reduced numbers of exchange pathways. Less structural order and fewer nearest neighbors lead to a canted or spin glass-like phase.[61–63] More recently, polarization-analyzed small-angle-neutron-scattering (PA-SANS) experiments on 9 nm diameter Fe_3O_4 particles indicate the presence of spin rearrangements in a core-shell motif.[64,65]

Since Mössbauer spectroscopy identified the presence of canted moments in spinel ferrites,[66] variable-field ^{57}Fe spectra were recorded for the coprecipitated and thermal decomposition cobalt ferrite samples studied herein (Figs. 6 and SM7). The field dependent spectra of both samples exhibit a significant decrease in the intensities of the $\Delta m_I = 0$ lines (2nd and 5th lines of the sextet pattern) (Fig. SM7). For a collection of randomly distributed iron sites with uniaxial magnetic properties, the relative intensities of the six lines are given by 3:2:1:1:2:3. However, when the applied field is parallel to the propagation direction of the 14.4 keV γ-rays, a finite angle θ between the applied field and the magnetization vector of the iron sites alters the intensity of the $\Delta m_I = 0$ lines, x, according to

$$x = \frac{4 \sin^2\theta}{(1 + \cos^2\theta)}. \tag{4}$$

Thus, the change in line intensities with the applied field is evidence of the field inducing a partial alignment of the moments associated with the individual lattices. Furthermore, the observation that, even at 80 kOe, the $\Delta m_I = 0$ lines of the two sextets have non-zero intensities indicates that the two samples exhibit a non-collinear arrangement of the local moments.[67–69] In a first approximation, the angle between the magnetization vectors of the two sublattices is ~142°. However, the data do not allow unambiguous deconvolution into bulk and surface components.

IV. DISCUSSION

The results from TEM, magnetometry, and Mössbauer studies indicate that samples **1** and **1a** are aggregated interacting nanoparticles, while sample **2** can be considered as single, or nearly single, domain weakly interacting particles. A potential cause for the change in coercivity with light is a change in volume of the magnetically ordered domains upon decoupling of the surface spins. According to Eq. (1), the energy barrier to spin reversal in a nanoparticle is proportional to the product of magnetocrystalline anisotropy and particle volume. If the absorption of light alters the coupling of the surface spins, the effective volume of the magnetic particle changes, decreasing the barrier to reversal. Assuming that the magnetocrystalline anisotropy does not change, a decrease in the coercivity of 0.58 kOe at 10 K for sample **2** can be accounted for by a 1.5% change in magnetic volume, corresponding to a 2–3 Å decrease in the magnetic particle diameter, little more than a surface layer or two. This mechanism is applicable below nominally 25 K. Above 25 K, such a transient, disequilibrium state is no longer able to be established, and the light induced changes in the magnetic response are governed by the competition between the magnetocrystalline anisotropy and the thermal energy, where the latter dominates above nominally 200 K.[70]

The magnitude of the photomagnetic response is much greater for the aggregates formed by the coprecipitation method, hinting of other intrinsic properties affecting the photomagnetism. The chemical composition, surface effects, and/or inter-particle interactions are some common factors that are expected to vary for the two samples based on their different synthesis conditions.[65,71,72] However, chemical analysis and site occupancy determined by XPS and Mössbauer spectroscopies indicate that the compositions are quite similar, suggesting that the different responses are not attributable to the chemical composition of the sample. The key difference is the extent of inter-particle interactions that are essentially absent in the thermal decomposition sample but dominate the magnetic properties of the coprecipitated sample. Particles within the aggregates experience dipolar coupling, but at the same time, they may also be physically connected. Modulation of the surface spins not only changes the magnetic volume but can also disrupt exchange coupling within aggregates, leading to an amplification of the light-induced effects.

Finally, we have also discovered a similar photomagnetic response in manganese ferrite isolated nanoparticles (Figs. SM4 and SM14 and associated text). Broadband irradiation of isolated, 4 nm manganese ferrite results in coercivity reduction from 105 Oe to 40 Oe and a significant high field magnetization drop below ~25 K, consistent with the energy scale identified in cobalt ferrite. These findings indicate that the photomagnetic response is not restricted to cobalt ferrite and is a general phenomenon in spinel ferrites.

V. CONCLUSIONS

In this work, we have examined photomagnetism in cobalt ferrite and observed several additional findings since the first report of photo-controlled magnetism in this material by Giri *et al.*[23,24] The broadband nature of the excitation that drives the light activated coercivity change and the presence of two energy scales, at ~25 K and ~200 K, suggests a complex underlying mechanism for the effect. In addition to the light-induced change in coercivity, which persists up to 200 K, a significant decrease in the high field magnetization upon light irradiation is observed below nominally 25 K.

Magnetometry and Mössbauer studies indicate that the high field magnetization behavior could be due to canted moments on the nanoparticles. Suppression of the magnetic contribution from the surface spins upon irradiation can yield a net reduction in the magnetic volume of the particle, contributing to the decrease in magnetization and coercive field. Furthermore, spin glass behavior and realignment of spins as a consequence of irradiation might also contribute. The study of cobalt ferrite prepared by two different synthesis protocols has revealed that the magnitude of the photomagnetic response is larger in aggregates of nanoparticles, where inter-particle interactions are important, while smaller in isolated nanoparticles.

The simplest description of the observations involves effective heating of the electronic bath of the surface spins, which are only weakly coupled to the lattice (phonon) reservoir below 25 K. At higher temperatures up to 200 K, the coupling between the two thermal reservoirs is intact, so the photo-perturbations of the spins are governed by the magneto-crystalline anisotropy of the lattice. Above 200 K, the phonon thermal energy dominates and the photo-induced changes of the magnetic response are no longer established. Although present in isolated nanoparticles, the effects are more extreme in aggregated ensembles as the irradiation primarily influences the surface spins, thereby interrupting magnetic cooperativity arising from the physical contact of the particles.

SUPPLEMENTARY MATERIAL

See supplementary material for particle size analyses of the samples investigated by TEM micrographs and XRD diffractograms, chemical analysis utilizing X-ray photoelectron spectroscopy (XPS) and Mössbauer spectroscopy, field and temperature dependences of spectra from Mössbauer spectroscopy, low temperature structural investigation of aggregated nanoparticles, temperature dependent magnetization of aggregates of nanoparticles, and light-induced magnetization changes in isolated manganese ferrite nanoparticles.

ACKNOWLEDGMENTS

[1]A. K. Zvezdin and V. A. Kotov, *Modern Magnetooptics and Magnetooptical Materials* (Taylor and Francis, 1997).
[2]A. Star, Y. Lu, K. Bradley, and G. Grüner, Nano Lett. **4**, 1587 (2004).
[3]J. Walowski and M. Münzenberg, J. Appl. Phys. **120**, 140901 (2016).
[4]M. H. Kryder, E. C. Gage, T. W. McDaniel, T. W. McDaniel, W. A. Challener, R. E. Rottmayer, G. Ju, Y.-T. Hsia, and M. F. Erden, Proc. IEEE **96**, 1810 (2008).
[5]C. D. Stanciu, F. Hansteen, A. V. Kimel, A. Kirilyuk, A. Tsukamoto, A. Itoh, and T. Rasing, Phys. Rev. Lett. **99**, 047601 (2007).
[6]C.-H. Hsia, T.-Y. Chen, and D. H. Son, Nano Lett. **8**, 571 (2008).
[7]A. Kirilyuk, A. V. Kimel, and T. Rasing, Rev. Mod. Phys. **82**, 2731 (2010).
[8]A. Kirilyuk, A. V. Kimel, and T. Rasing, Rep. Prog. Phys. **76**, 026501 (2013).
[9]C.-H. Lambert, S. Mangin, B. S. D. C. S. Varaprasad, Y. K. Takahashi, M. Hehn, M. Cinchetti, G. Malinowski, K. Hono, Y. Fainman, M. Aeschlimann, and E. E. Fullerton, Science **345**, 1337 (2014).
[10]S. Mangin, M. Gottwald, C.-H. Lambert, D. Steil, V. Uhlíř, L. Pang, M. Hehn, S. Alebrand, M. Cinchetti, G. Malinowski, Y. Fainman, M. Aeschlimann, and E. E. Fullerton, Nat. Mater. **13**, 286 (2014).
[11]W. D. Rice, P. Ambwani, M. Bombeck, J. D. Thompson, G. Haugstad, C. Leighton, and S. A. Crooker, Nat. Mater. **13**, 481 (2014).
[12]O. Sato, T. Iyoda, A. Fujishima, and K. Hashimoto, Science **272**, 704 (1996).
[13]P. Gütlich, Y. Garcia, and T. Woike, Coord. Chem. Rev. **219–221**, 839 (2001).
[14]O. N. Risset, P. A. Quintero, T. V. Brinzari, M. J. Andrus, M. W. Lufaso, M. W. Meisel, and D. R. Talham, J. Am. Chem. Soc. **136**, 15660 (2014).
[15]C. R. Gros, M. K. Peprah, B. D. Hosterman, T. V. Brinzari, P. A. Quintero, M. Sendova, M. W. Meisel, and D. R. Talham, J. Am. Chem. Soc. **136**, 9846 (2014).
[16]R. Bertoni, M. Lorenc, H. Cailleau, A. Tissot, J. Laisney, M.-L. Boillot, L. Stoleriu, A. Stancu, C. Enachescu, and E. Collet, Nat. Mater. **15**, 606 (2016).
[17]H. T. Lemke, K. S. Kjær, R. Hartsock, T. B. van Driel, M. Chollet, J. M. Glownia, S. Song, D. Zhu, E. Pace, S. F. Matar, M. M. Nielsen, M. Benfatto, K. J. Gaffney, E. Collet, and M. Cammarata, Nat. Commun. **8**, 15342 (2017).
[18]L. Bogani, L. Cavigli, C. de Julián Fernández, P. Mazzoldi, G. Mattei, M. Gurioli, M. Dressel, and D. Gatteschi, Adv. Mater. **22**, 4054 (2010).
[19]N. Al-Aqtash and R. Sabirianov, J. Mater. Chem. C **2**, 6873 (2014).
[20]M. Seki, A. A. Hossain, H. Tabata, and T. Kawai, Solid State Commun. **133**, 791 (2005).
[21]M. Seki, A. K. M. A. Hossain, T. Kawai, and H. Tabata, J. Appl. Phys. **97**, 083541 (2005).
[22]J. S. Bettinger, C. Piamonteze, R. V. Chopdekar, M. Liberati, E. Arenholz, and Y. Suzuki, Phys. Rev. B **80**, 140413 (2009).
[23]A. Giri, K. Pellerin, W. Pongsaksawad, M. Sorescu, and S. Majetich, IEEE Trans. Magn. **36**, 3029 (2000).
[24]A. K. Giri, E. M. Kirkpatrick, P. Moongkhamklang, S. A. Majetich, and V. G. Harris, Appl. Phys. Lett. **80**, 2341 (2002).
[25]S. Cojocaru and D. V. Anghel, Phys. Rev. B **93**, 115405 (2016).
[26]The time scale is certainly quicker than a few tens of seconds, which is required for making a magnetization measurement with our magnetometer, and presumably may extend down to the subpicosecond range.[7]
[27]L. B. Wang, O.-P. Saira, and J. P. Pekola, Appl. Phys. Lett. **112**, 013105 (2018).
[28]Z. Tang, C. Sorensen, K. Klabunde, and G. Hadjipanayis, J. Colloid Interface Sci. **146**, 38 (1991).
[29]Q. Song and Z. J. Zhang, J. Am. Chem. Soc. **126**, 6164–15137781 (2004).
[30]A. Lassenberger, T. A. Grünewald, P. D. J. van Oostrum, H. Rennhofer, H. Amenitsch, R. Zirbs, H. C. Lichtenegger, and E. Reimhult, Chem. Mater. **29**, 4511 (2017).
[31]C. A. Schneider, W. S. Rasband, and K. W. Eliceiri, Nat. Methods **9**, 671 (2012).
[32]D. Rancourt and J. Ping, Nucl. Instrum. Methods Phys. Res. Sect. B **58**, 85 (1991).
[33]A. Franco, F. L. A. Machado, and V. S. Zapf, J. Appl. Phys. **110**, 053913 (2011).
[34]E. J. W. Verwey, Nature **144**, 327 (1939).
[35]G. S. Parks and K. K. Kelley, J. Phys. Chem. **30**, 47 (1925).
[36]E. J. Samuelsen, E. J. Bleeker, L. Dobrzynski, and T. Riste, J. Appl. Phys. **39**, 1114 (1968).
[37]F. Walz, J. Phys.: Condens. Matter **14**, R285 (2002).

[38]F. Walz, V. A. M. Brabers, J. H. V. J. Brabers, and H. Kronmüller, J. Phys.: Condens. Matter **15**, 7029 (2003).

[39]J. García and G. Subías, J. Phys.: Condens. Matter **16**, R145 (2004).

[40]L. Chitu, M. Jergel, E. Majkova, S. Luby, I. Capek, A. Satka, J. Ivan, J. Kovac, and M. Timko, in *2006 Symposium A: Current Trends in Nanoscience-from Materials to Applications* [Mater. Sci. Eng.: C **27**, 1415 (2007)].

[41]J. Blasco, J. García, and G. Subías, Phys. Rev. B **83**, 104105 (2011).

[42]W. L. Peeters and J. W. D. Martens, J. Appl. Phys. **53**, 8178 (1982).

[43]J. Martens, W. Peeters, H. van Noort, and M. Erman, J. Phys. Chem. Solids **46**, 411 (1985).

[44]B. S. Holinsworth, D. Mazumdar, H. Sims, Q.-C. Sun, M. K. Yurtisigi, S. K. Sarker, A. Gupta, W. H. Butler, and J. L. Musfeldt, Appl. Phys. Lett. **103**, 082406 (2013).

[45]K. Sattler, in *Handbook of Thin Films*, edited by H. S. Nalwa (Academic Press, Burlington, 2002), pp. 61–97.

[46]P. Chen, X. Xu, C. Koenigsmann, A. C. Santulli, S. S. Wong, and J. L. Musfeldt, Nano Lett. **10**, 4526–20929203 (2010).

[47]Calculating the skin depth, $\delta = \sqrt{\rho/(\pi f \mu_r \mu_\circ)}$, involves the resistivity, ρ, relative permeability, μ_r, the frequency, f, and the permeability of the vacuum, $\mu_\circ$. The estimates of δ used $\rho = 2.5 \ \mu\Omega$ cm (Ref. 48) and $\mu_r = 7$.[49]

[48]G. Jonker, J. Phys. Chem. Solids **9**, 165 (1959).

[49]T. George, A. T. Sunny, and T. Varghese, IOP Conf. Ser.: Mater. Sci. Eng. **73**, 012050 (2015).

[50]A. López-Ortega, E. Lottini, C. d J. Fernández, and C. Sangregorio, Chem. Mater. **27**, 4048 (2015).

[51]E. S. Knowles, "Strain-mediated photomagnetic effects in heterostructured nanoparticles of Prussian blue analogues," Ph.D. thesis, University of Florida, 2013.

[52]S. Mørup, J. A. Dumesic, and H. Topsøe, in *Applications of Mössbauer Spectroscopy*, edited by R. L. Cohen (Academic Press, 1980) pp. 1–53.

[53]S. Mørup and M. F. Hansen, in *Handbook of Magnetism and Advanced Magnetic Materials*, edited by H. Kronmueller and S. Parkin (John Wiley and Sons, Ltd, 2007).

[54]P. Gütlich, E. Bill, and A. X. Trautwein, *Mössbauer Spectroscopy and Transition Metal Chemistry* (Springer-Verlag, 2011).

[55]W. F. Brown, Phys. Rev. **130**, 1677 (1963).

[56]D. Dickson, Hyperfine Interact. **111**, 171 (1998).

[57]S. Mørup and E. Tronc, Phys. Rev. Lett. **72**, 3278 (1994).

[58]M. Hansen and S. Mörup, J. Magn. Magn. Mater. **184**, L262 (1998).

[59]D. Peddis, C. Cannas, G. Piccaluga, E. Agostinelli, and D. Fiorani, Nanotechnology **21**, 125705 (2010).

[60]R. Aquino, J. Depeyrot, M. H. Sousa, F. A. Tourinho, E. Dubois, and R. Perzynski, Phys. Rev. B **72**, 184435 (2005).

[61]K. Haneda and A. H. Morrish, J. Appl. Phys. **63**, 4258 (1988).

[62]R. H. Kodama, A. E. Berkowitz, E. J. McNiff, Jr., and S. Foner, Phys. Rev. Lett. **77**, 394 (1996).

[63]M. P. Morales, S. Veintemillas-Verdaguer, M. I. Montero, C. J. Serna, A. Roig, L. Casas, B. Martínez, and F. Sandiumenge, Chem. Mater. **11**, 3058 (1999).

[64]K. L. Krycka, R. A. Booth, C. R. Hogg, Y. Ijiri, J. A. Borchers, W. C. Chen, S. M. Watson, M. Laver, T. R. Gentile, L. R. Dedon, S. Harris, J. J. Rhyne, and S. A. Majetich, Phys. Rev. Lett. **104**, 207203 (2010).

[65]K. L. Krycka, J. A. Borchers, R. A. Booth, Y. Ijiri, K. Hasz, J. J. Rhyne, and S. A. Majetich, Phys. Rev. Lett. **113**, 147203 (2014).

[66]S. Thakur, S. C. Katyal, A. Gupta, V. R. Reddy, S. K. Sharma, M. Knobel, and M. Singh, J. Phys. Chem. C **113**, 20785 (2009).

[67]A. Morrish and K. Haneda, J. Magn. Magn. Mater. **35**, 105 (1983).

[68]T. A. Anhöj, B. Bilenberg, B. Thomsen, C. D. Damsgaard, H. K. Rasmussen, C. S. Jacobsen, J. Mygind, and S. Mörup, J. Magn. Magn. Mater. **260**, 115 (2003).

[69]S. Mörup, in *Proceedings of the 4th International Conference on Fine Particle Magnetism (ICFPM)* [J. Magn. Magn. Mater. **266**, 110 (2003)].

[70]S. Yoon, J. Korean Phys. Soc. **59**, 3069 (2011).

[71]I. C. Nlebedim, Y. Melikhov, and D. C. Jiles, J. Appl. Phys. **115**, 043903 (2014).

[72]S. Bedanta and W. Kleemann, J. Phys. D: Appl. Phys. **42**, 013001 (2009).